

Research Article

Numerical Parametric Analysis of Similar Joints in Friction Stir Welding of Aluminum Alloy 6061-T6

A. Chogari¹, R. Beygi^{2*}, M.R. Sheykhosslami¹ and M. Shahsanami¹

¹ Department of Mechanical Engineering, Faculty of Engineering, Arak University, 38156-8-8349, Arak, Iran

² Department of Materials Science and Engineering, Faculty of Engineering, Arak University, 38156-8-8349, Arak, Iran

ARTICLE INFO

Article history:

Received 26 May 2024
Reviewed 05 June 2024
Revised 22 June 2024
Accepted 30 June 2024

Keywords:

Friction stir welding
Residual stress
Numerical modeling
Response surface method
Similar joint

Please cite this article as:

Chogari, A., Beygi, R., Sheykhosslami, M.R., & Shahsanami, M. (2024). Numerical parametric analysis of similar joints in friction stir welding of aluminum alloy 6061-T6. *Iranian Journal of Materials Forming*, 11(2), 4-14. <https://doi.org/10.22099/IJMF.2024.50103.1295>

ABSTRACT

Friction stir welding (FSW) is a solid-state welding technique that exhibits a lower residual stress compared to fusion welding. This study focuses on FE modeling of the process for homogeneous aluminum alloy 6061, presenting uncoupled thermal and mechanical analyses. The thermal analysis utilized a DFLUX subroutine, providing a reasonable temperature distribution that was validated experimentally through temperature measurement by mean of thermocouples. The computed temperature field was then incorporated into the mechanical analysis. To evaluate the impact of welding parameters including advancing speed and rotational speed on maximum welding temperature and residual stresses, an experimental design using the response surface method via Minitab Statistical Software 22 was employed. Results indicate that at a constant rotational speed, temperature and residual stress decrease at a constant advancing speed temperature by increasing the advancing speed while residual stress increases by increasing rotational speed.

© Shiraz University, Shiraz, Iran, 2024

1. Introduction

Friction stir welding (FSW) is a solid-state process that is widely used in different applications [1]. The general heat produced by the process remains below the melting temperature of the metal. This method involves a non-consumable spinning tool consisting of two parts: a shoulder and a pin. The spinning tool lowers into two

plates, which are firmly clamped on the backing plate until the tool shoulders touch the upper surfaces of the plates [2]. During the process, heat is generated due to the friction between the tool and the workpiece as well as through the plastic deformation of the material. The second function of the tool is "stirring" and "movement" of materials. Local heating softens the materials around

* Corresponding author

E-mail address: reza.beygi@gmail.com (R. Beygi)
<https://doi.org/10.22099/ijmf.2024.50103.1295>

the pin and the combination of tool rotation and tool translation results in the movement of materials from the front to the back of the spinning pin. As a result, the materials intermix locally and produce a 'solid-state' connection between the two plates while inducing local microstructural changes and residual stresses [3]. The primary reasons for using the FSW process include cost savings due to high strength, good repeatability, fine microstructure as well as excellent mechanical properties, and minimal distortion in the joints created by this process [4].

Aluminum alloy AA 6061-T6 is the most commonly used alloy in the 6000 series aluminum alloys. It exhibits favorable weldability properties compared to other aluminum alloys and is most widely used due to its corrosion resistance, high strength, and ease of machinability. It has become the preferred choice for use in FSW methods. AA 6061-T6 is particularly suitable for welding high-strength alloys commonly used in the automotive, aerospace and transportation industries [5, 6].

This process can join aluminum alloys without the melting stage, providing a joint with suitable physical and mechanical properties. There are several factors that influence the quality of the FSW joint including the rotational speed, tool feeding speed, the magnitude of downward force to maintain the stability between the tool and the workpiece, tool geometry, and tilt angle [7].

Welding residual stress is one of the critical parameters that can adversely affect the mechanical properties of the welded joint, leading to deformation, cracking, or fracture. Residual stresses created by welding result from non-uniform temperature changes, differential thermal expansion, and contraction between the weld metal and the base metal. The trend of recent studies in the field of residual stress in the FSW process is to introduce methods to reduce harmful residual stresses.

Nandan et al. [8] investigated the fundamental aspects of the FSW process and its metallurgical outcome, with a specific focus on heat generation, heat transfer, and plastic flow during welding. In a separate study, Song et al. [9] detailed the three-dimensional

transient heat transfer process in FSW using a mathematical model. This work involved both theoretical and experimental approaches. An explicit central differential scheme was employed to dynamically solve the control equations and the heat transfer during the three phases of welding, i.e. tool penetration, welding, and tool removal. The temperature variation during the welding was also measured to validate the calculated results. Zhang et al. [10] used a thermo-mechanical model to predict the temperature variations during the FSW process and investigated the effects of welding parameters on the temperature. A study on material flow patterns and residual stresses in the FSW process was also conducted by Zhang et al. [11]. In this study the distribution of longitudinal residual stress perpendicular to the weld line was investigated, which exhibited a double feature curve with its maximum increase associated with a rise in the translational velocity. Riahi et al. [12] developed a three-dimensional numerical simulation of FSW to investigate the effect of tool moving speed on heat distribution and residual stress. The obtained residual stress indicates that heat distribution varies along the thickness and is highly asymmetric. Furthermore, an increase in longitudinal residual stress in the weld occurred as the speed of the process and tool movement increased. In this study, only the thermal effect on the prediction of residual stress was investigated. Jafari et al. [13] determined residual stress distribution at the weld zone using the contour method. The residual stress distribution in the workpiece was found to be tensile in the centerline of the cut, and compressive on the edges. The highest residual stress value was 21.6% of the yield strength of the base AA 6061-T6 alloy. Khandkar et al. [14] employed a two-step simulation process to investigate the residual stresses generated during the thermal cycles of the FSW process on three different materials, AA 2024, AA 6061, and SS 304 L. A three-dimensional model using temperature-dependent material and thermo-physical properties was employed. The first simulation step is a thermal model that predicts the thermal history from an input torque, and the second is a mechanical model that predicts the residual thermal stresses based on the temperature

history generated by the thermal model. Feng et al. [15] employed an integrated thermal–metallurgical–mechanical model to analyze the residual stress and the changes in microstructure and properties of AA 6061-T6 friction stir welds. A three-dimensional finite element model was employed for simulation. It was observed that the distribution of residual stress in the FSW process is highly influenced by both the welding process parameters and the extent of material softening induced by welding. Buffa et al. [16] simulated the FSW process of butt joints employing a three-dimensional finite element model with general validity for different joint configurations through a single block approach. The model efficiently predicts residual stresses by considering thermal effects employing a novel and time-efficient approach. There is a good agreement between calculated and experimentally measured data. Ghahremani et al. [17] carried out metallographic analyses and mechanical studies on a friction stir welded plate made of AA 2024-T351 aluminum alloy with an 8 mm thickness. Both numerical and experimental findings indicated that an increase in traverse or rotational speed leads to an increase in the residual stress within the weld zone. In a study conducted by Sadeghi et al. [18], the main objective was the ultrasonic measurement of residual stresses through thickness in the FSW of aluminum plates. A three-dimensional thermo-mechanical finite element analysis was utilized to predict the residual stresses resulting from the FSW of 5086 aluminum plates. Sun et al. [19] analyzed the deformation characteristics of a friction stir welded thin sheet aluminum alloy joint using numerical simulations and experimental results. Stress analysis revealed a high-stress region at the weld's end, mainly from shear stress in the x-y direction. Thermal analysis and optimization of FSW AA 6061 alloy joints at various welding speeds, rotational speeds, and tool geometry was examined by Maleku et al. [20]. The temperature range for welding was found via software simulation. Experimental work validated the temperature value obtained from finite element analysis.

The current study has aimed to analyze the temperature distribution and longitudinal and transverse

residual stresses during the FSW of two aluminum 6061-T6 plates using the finite element method. Experimental tests were conducted to validate the accuracy of the temperature distribution calculated through numerical analysis. In the subsequent phase, the welding residual stresses were determined using an uncoupled mechanical model. The impact of rotating speed and advancing speed on both temperature and residual stresses is then investigated through a design of experiments.

2. Simulation Procedure

A three-dimensional finite element model was considered in Abaqus 2017 to numerically simulate the FSW process using an uncoupled thermo-mechanical solution. Because of the symmetrical geometry and boundary conditions, half of the workpiece was modeled to reduce the calculation time. The model did not contain the tool. The tool effect on the temperature rise was considered by applying an appropriate heat flux model. The type of element chosen for the thermal solution was the linear heat transfer element DCD8. The geometry of this element is a cube with eight nodes, which is deemed adequate for heat transfer simulations in Abaqus. The linear 3D stress element C3D8R, configured as a cube with eight nodes, was selected for mechanical simulation. Additionally, for optimizing the element quantities and reducing the solution time, non-uniform meshing across the width of the workpiece and higher mesh density along the weld line were considered. A mesh size independent study was used to determine the element size of both the thermal and mechanical simulations.

In order to simulate experimental data, the properties of aluminum alloy 6061-T6 were used as temperature-dependent. The properties of material at different temperatures are shown in Table 1.

2.1. Thermal analysis

In the thermal analysis, two distinct solution steps should be done: One is related to the welding process and the other to cooling the piece. The welding process step time is determined based on the tool's linear speed. In the

Table 1. Properties of AA 6061-T6 at different temperatures [21]

Temperature (°C)	Density (kg/m ³)	Conductivity (W/m.°C)	Specific heat (J/kg.°C)	Young's modulus (GPa)	Poisson's ratio	Expansion coefficient (μ/°C)	Yield strength (MPa)
25	2700	167	896	68.9	0.33	22	267
37.8	2685	170	945	68.54	0.33	23.45	274.4
93.3	2685	177	978	66.19	0.33	24.61	264.6
148.9	2667	184	1004	63.09	0.33	25.67	248.2
204.4	2657	192	1028	59.16	0.33	26.6	218.6
260	2657	201	1052	53.99	0.33	27.56	159.7
315.6	2630	207	1078	47.48	0.33	28.53	66.2
371.1	2630	217	1104	40.34	0.33	29.57	34.5
426.7	2602	223	1133	31.72	0.33	30.71	17.9

cooling step, initiated after welding, the step time is the time required for the piece to reach room temperature.

To apply the heat generated from tool-induced friction and plastic flow directly to the workpiece the heat flux model by Schmidt and Hattel's [22] was employed within an appropriate subroutine.

In this model, heat production sources are heat generated by the tool shoulder and the heat produced by the tool pin. Four distinct regions can be recognized as heat-producing zones when the tool penetrates the workpiece. The heat generated in these regions can be assigned to the frictional interaction between the tool and the workpiece.

The first region, which generates the majority of the heat, is the tool shoulder. The second one involves the heat produced by the walls and the periphery of the pin, and the other region pertains to the pin's bottom.

In this paper, the heat flux generated from the shoulder and generated from the pin were distinctly separated. The surface flux and the volume flux were employed to apply the heat fluxes associated with these regions. A heat flux is applied to the upper surface of the workpiece, representing the heat generated by the tool shoulder. Another distinct heat flux is applied to the volume of the piece, signifying the heat generated by the pin [23]. The heat produced by the tool shoulder and the heat generated by the tool pin are expressed as Eq. (1) and Eq. (2):

$$Q_{shoulder} = \frac{2\pi\omega\mu P}{3}(R_1^3 - R_2^3) \quad (1)$$

$$Q_{pin} = Q_{pinprofile} + Q_{pinbottom} = 2\pi\mu\omega PR_2^2 H + \frac{2\pi\omega\mu P}{3} R_2^3 \quad (2)$$

Where ω is the tool angular velocity, μ is the friction coefficient that is approximately 0.4, P is the force applied to the workpiece (4000 N), R_1 is the tool shoulder radius and R_2 is the pin radius, and H is the height of the pin. In these equations, heat is expressed in Joules.

Following the calculation of the heat from the shoulder and the pin, the shoulder heat must be divided by the surface area of the shoulder and the pin heat by the volume of the pin before introducing the heat flux into Abaqus [24].

These two heat fluxes are only applied to the workpiece during the welding solution step and should be deactivated in the cooling solution step to carry out the cooling process.

Using the DFLUX subroutine, it is possible to define a heat flux or mass flux (whether on the surface or volume) as a function of parameters such as time, temperature, etc.

2.2. Mechanical analysis

The mechanical simulation was then carried out using the temperature distribution obtained from thermal analysis as the input condition. A static general module was employed for mechanical simulation with the step time equal to the sum of the welding and cooling steps from the thermal analysis.

2.3. Boundary conditions

For thermal simulation, the Stefan-Boltzmann constant for zero absolute temperature (-273 °C), room temperature of 25 °C, and an emissivity coefficient of 0.6 are boundary conditions for radiation. The

convective heat transfer coefficient equal to $30 \text{ W}/(\text{m}^2 \cdot ^\circ\text{C})$ and an ambient temperature of $25 \text{ }^\circ\text{C}$ are boundary conditions for convection. These conditions were assigned to the contact sections between the workpiece and air.

Two plates are firmly clamped on the backing plate during welding to prevent buckling caused by the tool pressure. A virtual displacement boundary condition with a heat transfer coefficient of $350 \text{ W}/(\text{m}^2 \cdot \text{K})$ [23] was defined for the anvil and the sub-section of the workpiece in simulation for modeling these plates. In addition, all degrees of freedom for the outer edge of the plate were fixed. The numerical model did not contain the tool, so no defined contact boundary condition existed for the tool. Half of the workpiece was modeled in the numerical study, so a symmetrical boundary condition about the Z-axis was necessary for the inner edge of the plate.

3. Experimental Verification

For the experimental verification of the numerical model, two $130 \times 50 \times 3 \text{ mm}$ AA 6061-T6 plates were used that were workpieces for a similar FSW process. After the preparation of the samples, a hole was drilled in the middle section of the piece, 20 millimeters away from the weld line, to accommodate the thermocouple. The tool geometry was simple cylindrical and made of hot-work steel H13. The tool had a 12 mm shaft diameter, 3 mm pin diameter, and 2.8 mm pin length. A steel plate was the backing plate on the base of the milling machine. Workpieces were fixed during welding with the four-component fixture. To measure the temperature during welding, a microprocessor-controlled thermostat model MMX-400PI with the capability to measure temperatures between 50 to $400 \text{ }^\circ\text{C}$ with a resolution of 1 degree was utilized. A wired thermocouple was fabricated in the central section of the workpiece to record the temperature. Fig. 1 shows the FSW machine in the experiments. In this device, the rotational speed of the spindle was 1100 rev/min in a clockwise direction, and its linear motion was manually adjusted.



Fig. 1. Experimental setup.

4. Design of Experiments (DOE)

A statistical approach based on the response surface method (RSM) was used to study the effect of various welding parameters, including advance speed and rotational speed, on the workpiece temperature, and longitudinal and transverse residual stresses in the FSW process. Repetitive samples in the DOE assess the repeatability and validation of the designed model. The tool's rotational speed ranged from 600-1200 rev/min with increments of 300 rev/min, and its linear speed ranged from 20-200 mm/min with increments of 90 mm/min.

5. Results and Discussion

5.1. Heat distribution and validation

In order to validate the numerical model, the temperature was recorded and subsequently compared with the thermal section of the numerical model. A rotational speed of 1100 rev/min, equivalent to 115.19 rad/s, and a linear speed of 34 mm/min, corresponding to 0.00056 m/s, were applied in accordance with the milling machine and its tool settings, in the experimental work within the DFLUX subroutine code.

Welding at a linear speed of 34 mm/min was performed over a length of 60 mm. To implement this, the starting point coordinates in the subroutine code were considered at 35 mm from the beginning of the workpiece.

The maximum temperature recorded by the monitoring system during the experimental test as depicted in Fig. 2 has been 200 °C. Fig. 3 depicts temperature profiles extracted from the numerical model and Abaqus software in a distance of 20 mm away from the weld line.

The maximum predicted temperature at this point is 261 degrees. The 30% discrepancy between the obtained results can be attributed to variations in boundary conditions between the modeling and experimental tests, uncertainty of material properties, and the absence of tool modeling demonstrating the reliability of the modeling with a reasonable approximation. In numerical modeling, the temperature reaches 589 degrees in the weld region, gradually decreasing as it moves away from this area.

The temperature increase trend in the weld region is such that as the tool approaches that area, the temperature of that section rises steeply, and after the tool passes, it decreases with the same slope. However, the cooling process and reaching ambient temperature occur gradually with a gentle slope, requiring more time.

After validating the simulation procedure, the temperature distribution can be obtained for any other plate and pin dimensions. The model length and width were 145 mm and 75 mm, and the thickness was 6.35 mm. The cylindrical pin had a radius of 9.35 mm.

As depicted in Fig. 4, the temperature distribution in

section A-A, located at the midpoint of the piece and perpendicular to the welding direction, conforms to a V-shaped welding section. The asymmetric temperature distribution is attributed to a relatively higher convection coefficient on the lower surface of the workpiece (350 W/m².K) compared to the upper surface (30 W/m².K). Operating at a linear tool speed of 280 mm/min and a rotational speed of 1250 rev/min, the elevated temperature in the welding zone results from the friction between the tool shoulder and the workpiece surface, coupled with intense plastic deformation in this region. Moving away from this region results in a gradual decrease in temperature. The maximum temperature is predicted 527 °C in the region under the shoulder on the top surface, while the solidus temperature of AA 6061 is 582 °C.

5.2. Residual stresses

Using the mechanical model, longitudinal and transverse residual stresses in the workpiece after complete cooling of the plates in the middle section of them were

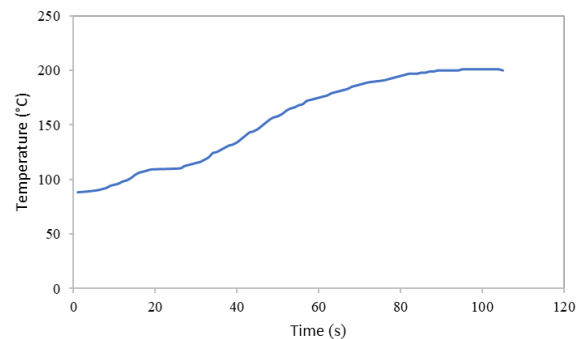


Fig. 2. Temperature recorded by monitoring system during the experimental test.

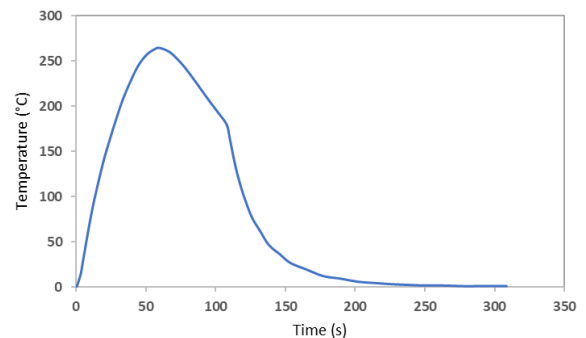


Fig. 3. Time-temperature diagram extracted from numerical analysis.

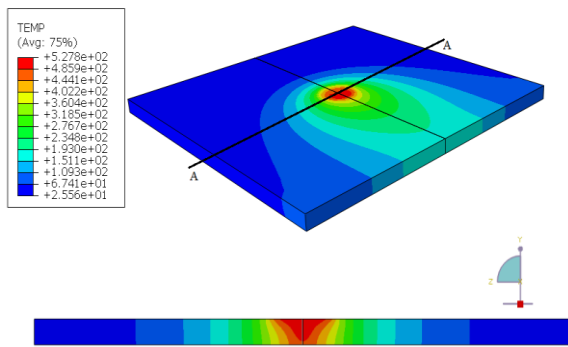


Fig. 4. Temperature distribution in the A-A cross-section perpendicular to the weld center line.

5.2. Residual stresses

Using the mechanical model, longitudinal and transverse residual stresses in the workpiece after complete cooling of the plates in the middle section of them were determined with welding speed of 280 mm/min and rotational speed of 1250 rev/min.

The longitudinal and transverse residual stresses from the finite element model are depicted in Fig. 5, which illustrates the distribution of stresses on the middle surface of the workpiece after cooling and reaching room temperature. It indicates that the longitudinal residual stress in the weld region is entirely tensile. Additionally, the region under the tool shoulder exhibits the highest residual stress.

Fig. 6 depicts longitudinal and transverse stress residual stress following the completion of the welding as well as the completion of the cooling process. The joint edge of the plates exhibits the highest longitudinal stress which is less than their yield stress. In the transverse stress, some localized points approach the yield stress resulting in localized yield phenomena that are subsequently corrected.

6. Design of Experiment Results

To optimize the process and evaluate the impact of various welding parameters, including traverse speed and rotational speed, an experiment was designed using Minitab Statistical Software 22, considering different rotational and linear speeds. This experiment aims to determine the effect of these parameters on the maximum temperature. Repeated samples were taken

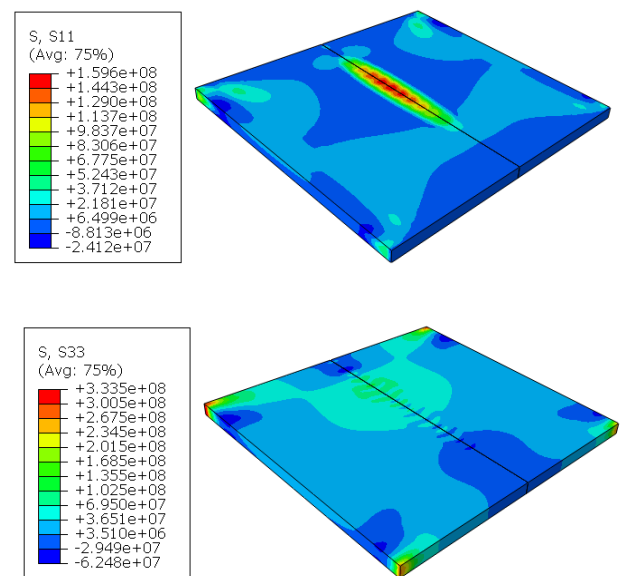


Fig. 5. longitudinal (S11) and transverse (S33) stress profiles in middle surface of the workpiece.

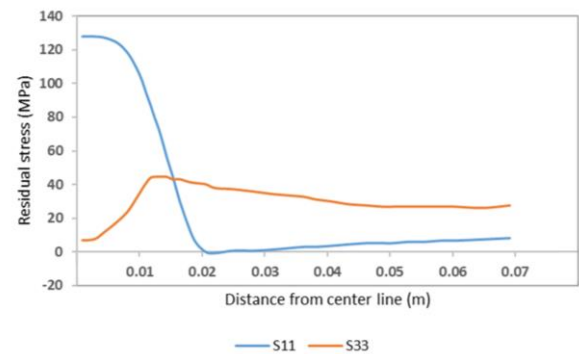


Fig. 6. Longitudinal (S11) and transverse (S33) residual stress distribution in the workpiece following the cooling process.

into account to assess the repeatability and validate the designed model. The data from this experiment is presented in Table 2. In order to simulate the experimental data, the temperature-dependent properties of the aluminum alloy 6061-T6 as specified in Table 1 were used. The dimensions of the workpiece were 130×50×3 mm, and a simple cylindrical tool with a shoulder diameter of 12 mm, a pin diameter of 3 mm, and a pin height of 2.8 mm were considered.

Fig. 7 depicts the temperature variations with different rotational and transverse speeds. The impact of rotational speed is much greater than the impact of advancing speed on the maximum temperature in the welding zone.

Table 2. Design of experiment based on different linear and transverse speed

Number of experiments	1	2	3	4	5	6	7	8	9	10	11	12	13
Linear speed (mm/min)	20	110	200	200	20	20	110	110	110	200	110	110	110
Rotational speed (rpm)	1200	900	600	1200	600	900	900	600	900	900	1200	900	900

The maximum temperature (651 °C) was observed in a sample with a rotational speed of 1200 rev/min and a linear speed of 20 mm/min and the minimum temperature (308 °C) was observed in a sample with a rotational speed of 600 rev/min and a linear speed of 200 mm/min.

The results of the thermal and mechanical numerical modeling were expressed based on the values of the experimental design.

By comparing graphs in Fig. 8, it can be observed that at a constant rotational speed, the welding zone temperature decreases by increasing the advancing speed due to the fact that the materials have less time for mixing and temperature increase. By comparing graphs in Fig. 9, it can be observed that at a constant advancing speed the welding zone temperature increases by increasing the rotational speed, the reason being an increase in the friction and, consequently, more material mixing.

Another important point that can be observed from the comparison of temperature graphs is that, at a constant rotational speed, an increase in advancing speed leads to a more uniform decrease in the temperature difference between the welding zone and the base metal.

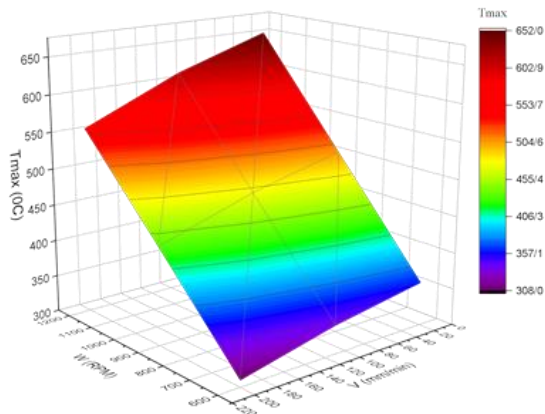


Fig. 7. Maximum temperature distribution with different rotational and transverse speeds.

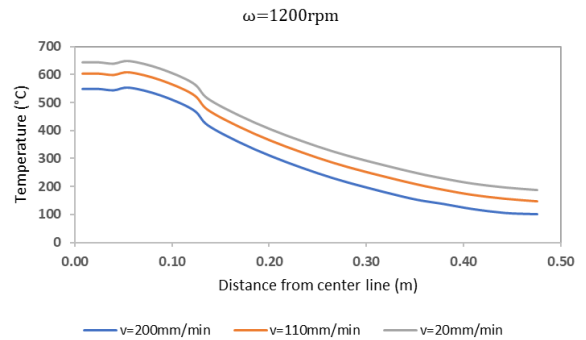


Fig. 8. Variation of temperature in the cross section of the weld at different advancing speed with rotation speed of 1200 rpm.

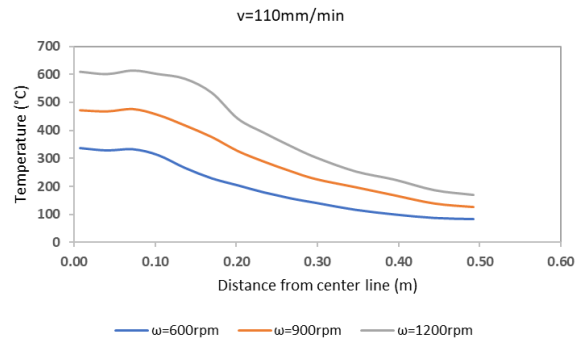


Fig. 9. Variation of temperature in the cross section of the weld at different rotation speeds with advancing speed of 110 mm/min.

However, at a constant advancing speed, an increase in the rotational speed results in a greater increase in the maximum temperature in the welding zone compared to the base metal.

Subsequently, the residual stresses results were expressed based on the experimental design. Initially longitudinal stresses were considered. As depicted in Fig. 10, it can be observed that at a constant rotational speed, the longitudinal residual stresses under tool shoulder decreases after cooling down the work piece and reaching ambient temperature by increasing the advancing speed.

Upon comparing graphs in Fig. 11, it is evident that

at a constant advancing speed, the longitudinal residual stresses under tool shoulder increases after cooling the work piece and reaching an ambient temperature by increasing the rotational speed. Then, the change in the trend of transverse stress variations was considered. At a constant rotational speed, by increasing advancing speed, the transverse residual stresses under tool shoulder decreases after cooling down the work piece and reaching ambient temperature. In addition, at a constant advancing speed, the transverse residual stresses under tool shoulder decreases following cooling the work piece and reaching ambient temperature with increasing rotational speed.

In general, at a constant rotational speed, an increase in the advancing speed leads to a reduction in residual stresses, while at a constant advancing speed, an increase in rotational speed results in an elevation of residual stresses.

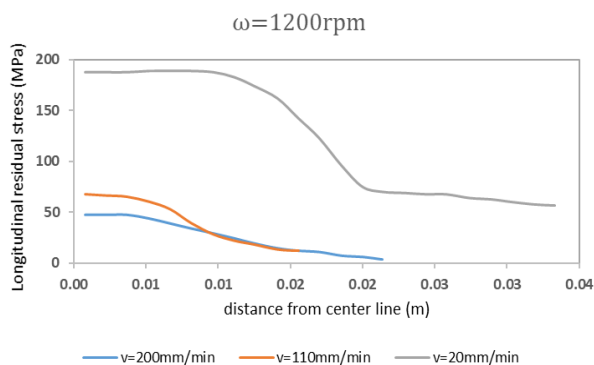


Fig. 10. Variation of longitudinal residual stress at different advancing speed with rotation speed of 1200 rpm.

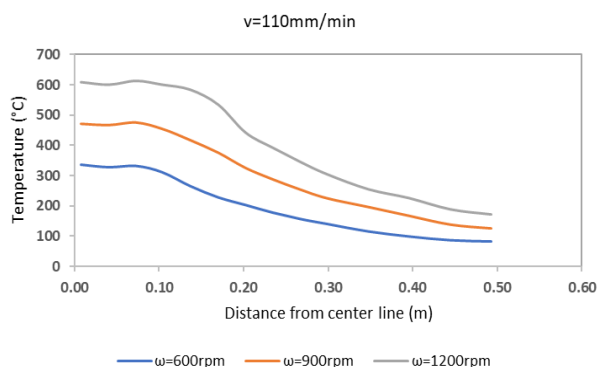


Fig. 11. Variation of stress at different rotating speed with advancing speed of 110 mm/min.

7. Conclusion

A numerical thermal and mechanical modeling of the FSW process for homogenous aluminum alloy 6061, utilizing a simple cylindrical tool was conducted. The accuracy of the thermal model was verified through experimental tests performed on the FSW machine. The uncoupled analysis approach involved two distinct thermal and mechanical solution steps for which the temperature distribution predicted by the numerical model was effectively validated against real-time temperature data recorded by a monitoring system. The results revealed a 30% discrepancy between the predicted maximum temperature and the maximum temperature recorded by the monitoring system. This deviation can be attributed to differences in boundary conditions between the modeling and experimental tests, the absence of tool modeling, uncertainties in material properties, and heat losses during the experimental setup.

Subsequently, an experimental design was implemented to investigate the influence of varying advancing and rotational speeds on welding temperature and residual stresses. The maximum temperature (651 °C) was observed in a sample with a rotational speed of 1200 rev/min and a linear speed of 20 mm/min. The minimum temperature (308 °C) was observed in a sample with a rotational speed of 600 rev/min and a linear speed of 200 mm/min. Conversely, at a constant advancing speed, an increase in rotational speed resulted in elevated welding temperature as well as longitudinal and transverse residual stresses. The maximum longitudinal stress (190 MPa) was observed in a sample with a rotational speed of 1200 rev/min and a linear speed of 20 mm/min and the minimum longitudinal residual stress (6 MPa) was observed in a sample with a rotational speed of 600 rev/min and a linear speed of 200 mm/min. The impact of rotational speed on welding temperatures was found to be significantly greater than that of the effect of advancing speed.

Conflict of Interest

There is no conflict of interest.

Funding

There is no funding available.

8. References

- [1] Lohwasser, D., & Chen, Z. (Eds.). (2009). *Friction stir welding: From basics to applications*. Elsevier.
- [2] Cho, J. H., Boyce, D. E., & Dawson, P. R. (2005). Modeling strain hardening and texture evolution in friction stir welding of stainless steel. *Materials Science and Engineering: A*, 398(1-2), 146-163. <https://doi.org/10.1016/j.msea.2005.03.002>
- [3] London, B., Mahoney, M., Bingel, W., Calabrese, M., & Waldron, D. (2001). Experimental methods for determining material flow in friction stir welds. In *The Third International Symposium on Friction Stir Welding*, Kobe, Japan (Vol. 27, p. 28).
- [4] Mishra, R. S., & Ma, Z. Y. (2005). Friction stir welding and processing. *Materials Science and Engineering: R: Reports*, 50(1-2), 1-78. <https://doi.org/10.1016/j.mser.2005.07.001>
- [5] Ajri, A., Rohatgi, N., Shin, Y. C. (2020). Analysis of defect formation mechanisms and their effects on weld strength during friction stir welding of Al 6061-T6 via experiments and finite element modeling. *The International Journal of Advanced Manufacturing Technology*, 107, 4621-4635. <https://doi.org/10.1007/s00170-020-05353-3>
- [6] Asmare, A., Al-Sabur, R., Messele, E. (2020). Experimental investigation of friction Stir welding on 6061-T6 aluminum alloy using Taguchi-based GRA. *Journal of Metals*, 10(11), 1480. <https://doi.org/10.3390/met10111480>
- [7] Uday, M. B., Ahmad Fauzi, M. N., Zuhailawati, H., & Ismail, A. B. (2010). Advances in friction welding process: a review. *Science and Technology of Welding and Joining*, 15(7), 534-558. <https://doi.org/10.1179/136217110X12785889550064>
- [8] Nandan, R., DebRoy, T., & Bhadeshia, H. K. D. H. (2008). Recent advances in friction-stir welding—process, weldment structure and properties. *Progress in Materials Science*, 53(6), 980-1023. <https://doi.org/10.1016/j.pmatsci.2008.05.001>
- [9] Song, M., & Kovacevic, R. (2003). Numerical and experimental study of the heat transfer process in friction stir welding. *Proceedings of the Institution of Mechanical Engineers, Part B: Journal of Engineering Manufacture*, 217(1), 73-85. <https://doi.org/10.1243/095440503762502297>
- [10] Zhang, Z., & Zhang H. W. (2009). Numerical studies on controlling of process parameters in friction stir welding. *Journal of Materials Processing Technology*, 209(1), 241-270. <https://doi.org/10.1016/j.jmatprotec.2008.01.044>
- [11] Zhang, H. W., Zhang, Z., & Chen, J. T. (2005). The finite element simulation of the friction stir welding process. *Materials Science and Engineering: A*, 403(1-2), 340-348. <https://doi.org/10.1016/j.msea.2005.05.052>
- [12] Riahi, M., & Nazari, H. (2011). Analysis of transient temperature and residual thermal stresses in friction stir welding of aluminum alloy 6061-T6 via numerical simulation. *The International Journal of Advanced Manufacturing Technology*, 55(1), 143-152. <https://doi.org/10.1007/s00170-010-3038-z>
- [13] Jafari, H., Mansouri, H., & Honarpisheh, M. (2019). Investigation of residual stress distribution of dissimilar Al-7075-T6 and Al-6061-T6 in the friction stir welding process strengthened with SiO₂ nanoparticles. *Journal of Manufacturing Processes*, 43, 145-153. <https://doi.org/10.1016/j.jmapro.2019.05.023>
- [14] Khandkar, M. Z. H., Khan, J. A., Reynolds, A. P., & Sutton, M. A. (2006). Predicting residual thermal stresses in friction stir welded metals. *Journal of Materials Processing Technology*, 174(1-3), 195-203. <https://doi.org/10.1016/j.jmatprotec.2005.12.013>
- [15] Feng, Z., Wang, Z. L., David, S. A., & Sklad, P. S. (2007). Modelling of residual stresses and property distributions in friction stir welds of aluminium alloy 6061-T6. *Science and Technology of Welding and Joining*, 12(4), 348-356. <https://doi.org/10.1179/174329307X197610>
- [16] Buffa, G., Ducato, A., & Fratini, L. (2011). Numerical procedure for residual stresses prediction in friction stir welding. *Finite Elements in Analysis and Design*, 47(4), 470-476. <https://doi.org/10.1016/j.finel.2010.12.018>
- [17] Ghahremani-Moghadam, D., Farhangdoost, K., & Masoudi Nejad, R. (2016). Microstructure and residual stress distributions under the influence of welding speed in friction stir welded 2024 aluminum alloy. *Metallurgical and Materials Transactions B*, 47(3), 2048-2062. <https://doi.org/10.1007/s11663-016-0611-3>
- [18] Sadeghi, S., Ahmadi Najafabadi, M., Javadi, Y., & Mohammadisefat, M. (2013). Using ultrasonic waves and finite element method to evaluate through-thickness residual stresses distribution in the friction stir welding of aluminum plates. *Materials & Design (1980-2015)*, 52, 870-880. <https://doi.org/10.1016/j.matdes.2013.06.032>
- [19] Sun, H., Zhou, Q., Zhu, J., Shi, X., Sun, Z. (2020). Deformation analysis of a friction stir-welded thin sheet aluminum alloy joint. *China Welding*, 29(1), 56-62. <https://doi.org/10.12073/j.cw.20190902002>
- [20] Melaku, L. E., Tura, A. D., Mamo, H. B., Santhosh, A. J., Ashok, N. (2022). Optimization and thermal analysis of friction stir welding on AA6061 aluminum alloys. *Materials Today: Proceedings*, 65(8), 3348-3356. <https://doi.org/10.1016/j.matpr.2022.05.463>

- [21] Chao, Y. J., & Qi, X. (1998). Thermal and thermo-mechanical modeling of friction stir welding of aluminum alloy 6061-T6. *Journal of Materials Processing & Manufacturing Science*, 7(2), 215-233.
<https://doi.org/10.1106/LTKR-JFBM-RGMV-WVCF>
- [22] Schmidt, H. N. B., Hattel, J., & Wert, J. (2004). An analytical model for the heat generation in friction stir welding. *Modelling and Simulation in Materials Science and Engineering*, 12(1), 143-157.
<https://doi.org/10.1088/0965-0393/12/1/013>
- [23] Ji, S. D., Jin, Y. Y., Yue, Y. M., Gao, S. S., Huang, Y. X., & Wang, L. (2013). Effect of temperature on material transfer behavior at different stages of friction stir welded 7075-T6 aluminum alloy. *Journal of Materials Science & Technology*, 29(10), 955-960.
<https://doi.org/10.1016/j.jmst.2013.05.018>
- [24] Chao, Y. J., Qi, Z., & Tang, W. (2003). Heat transfer in friction stir welding—experimental and numerical studies. *Journal of Manufacturing Science and Engineering*, 125(1), 138-145.
<https://doi.org/10.1115/1.1537741>